Rate dependency and ply thickness influence on transverse cracking evolution in cross-ply laminates

Fabien Coussa, Julien Berthe, Matthieu Ragonet

Rate dependency and ply thickness influence on transverse cracking evolution in cross-ply laminates

Fabien Coussa[1], **Julien Berthe**[1,2], **and Matthieu Ragonet**[1]

[1] ONERA, Materials and Structures Department / Design & Dynamic Resistance Research Unit - 5 rue des Fortifications, CS 90013, 59045 Lille Cedex - France
[2] Univ. Lille, CNRS, Centrale Lille, UMR 9013 - LaMCube, Laboratoire de Mécanique, Multiphysiques, Multiéchelles, F-59000 Lille - France
[1] Correspondance: fabien.coussa@onera.fr / julien.berthe@onera.fr

In this study, the rate dependency of transverse cracking evolution in cross-ply laminates is investigated for several 90° plies thicknesses. The crack detection methodology is based on a recently proposed protocol relying on the use of infrared thermography. A new analysis methodology is proposed to make it more robust and to directly link the spatial localization of the crack with the stress level at which it occurs. Based on this methodology, the results obtained for various loading rates and 90° ply thicknesses are analysed. The crack density evolution with respect to stress apply to the laminate exhibits a rate dependency only for the $[0/90]_S$ configuration. This rate dependency is finally discussed based on transverse crack onset theories in cross-ply laminates.

Keywords Transverse cracking, Rate dependency, Infrared thermography, Composite materials

1 Introduction

The increased use of composite materials in the transport industries and in applications to structural parts has led to the use of a wide range of experimental techniques to analyse the evolution of the degradation mechanisms by matrix cracking under different kinds of loadings. In the range of low and quasi-static loading rates, the analysis of the cracking density in cross-ply laminate has been the subject of numerous studies: Crossman et al. 1980; Dzenis 2003; Farge et al. 2010. Most of these techniques have been used under cyclic loadings where the interruption of the test allows the observation and the measurement of the material degradation mechanisms for various loading levels. For the dynamic speed range, however, the use of such protocols is limited due to the open-loop control of the testing machine. Difficulties related to the interruption of loading before the specimen failure is still considered as a real limit to this kind of analysis. In this work, in order to analyse the effect of the loading-rate increase on the evolution of the cracking density as a function of the applied stress, a non-intrusive measurement technique using infrared (IR) thermography is used. This approach has been used to measure the evolution of damage in composites submitted to quasi-static loadings (Lisle et al. 2013; Montesano et al. 2014), fatigue loadings (Toubal et al. 2006; Li et al. 2016) and more recently to loadings at intermediate dynamic loading-rate (Battams et al. 2016). Nevertheless, the detection and the quantification by IR thermography of transverse cracks for dynamic loads remains few investigated in the literature due to the limitations related to the acquisition frequency of the older generation of IR cameras. This work proposes to extend the analysis performed in the quasi-static ranges in Berthe et al. 2018 to a dynamic loading-rate range, through the use of a high rate IR camera (Telops FAST M3K).

In the sequel, the experimental procedure is first introduced in order to present the material of the study and the experimental setup. Thus, an innovative analysis procedure is proposed and applied on tests performed at various loading rates. Finally, this procedure is applied on the experimental results to analyse the loading-rate influence for various 90° ply thicknesses.

2 Experimental procedure

2.1 Material and specimens

The material considered in this study is the unidirectional prepreg HexPly M21/35%/268/T700GC (Hexcel France) made of T700 carbon fibres and the M21 epoxy resin. The impact resistance performance of this material has been enhanced by means of the inclusion of thermoplastic nodules in the epoxy resin. Laminate plates have been manufactured by hand lay-up. A typical cure cycle has been performed in an autoclave. Different symmetric and balanced stacking sequences have been chosen: $[0/90_3]_S$, $[0/90_2]_S$, $[0/90]_S$ and $[0/90_{1/2}]_S$. Rectangular specimens were cut out of plates using a water-cooled diamond saw with the following dimensions: 15 mm wide and a free length l_0 of 41 mm between the GFRP tabs with an approximate length of about 50 mm. The different specimen thicknesses are respectively associated with the different stacking sequences as follows: 2.15 mm, 1.61 mm, 1.08 mm and 0.81 mm.

2.2 Test setup

The experimental environment for the whole experimental investigation is illustrated in Figure 1. Every

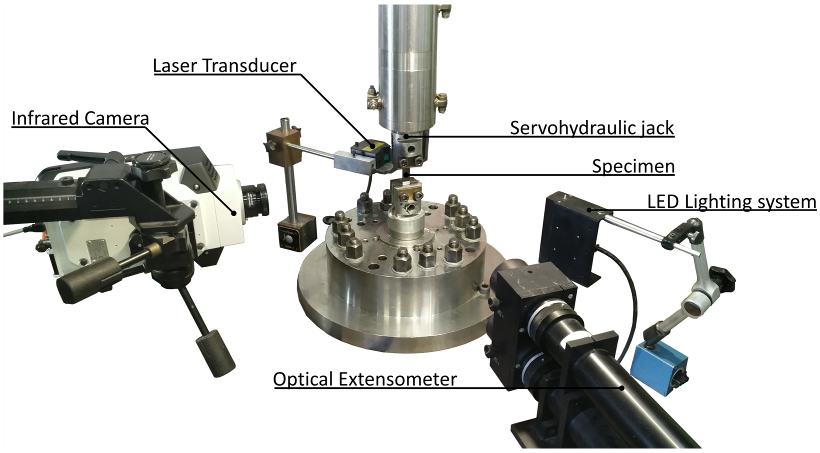

Figure 1: Experimental set-up suitable for the static and dynamic strain-rate range

tests have been performed by means of the use of a SCHENCK servohydraulic jack. This test facility allows to apply on the specimen various constant upper holder speeds from 5 mm.min^{-1} to 10 m.s^{-1}. This study is focused on five different upper holder speeds: 5 mm.min^{-1}, 50 mm.min^{-1}, 500 mm.min^{-1}, 0.1 m.s^{-1} and 1.4 m.s^{-1}. The objective is to finely cover a wide range of theoretical strain-rates from quasi-static range of $\dot{\varepsilon}$ = 2.10^{-3} s^{-1} to an intermediate dynamic range of $\dot{\varepsilon}$ = 35 s^{-1}. The measurement of the applied load is performed by a Kistler piezoelectric load-cell (Kistler 9071A). A pre-loading has been applied in order to be able to measure loads between -200 kN and +200 kN. The measurement of the upper holder displacement is performed by means of a Keyence laser transducer (Keyence LK-HD500 and LK-H052) in order to be able to accurately capture the real speed applied to the specimen. The specimen longitudinal strain is measured using a non-contact technique to avoid any disturbance of the measurement that could be generated by the appearance of cracks (Berthe et al. 2018). An optical extensometer Rudolph 200XR is used to capture two black-and-white transitions painted on the specimen surface. The two transitions are separated by a distance l of about 32 mm. The distance l has been precisely measured for each specimen before each test. At last, a Telops Fast M3k infrared camera with a 50-mm lens is used to monitor the temperature evolution of the edge surface of the free length of the samples. The camera sensor allows to capture an image of 320×256 pixesl up to 3.1 kHz in full frame an up to 100 kHz with a reduced spatial resolution of 64×4 pixels. Transverse crack propagation in $[0_m/90_n]_s$ can be considered as instantaneous from side to side (Berthelot 2003; Huchette 2005). This hypothesis remains valid with the loading rate increase (Berthe et al. 2018). Based on this assumption, only one edge of the different specimens has been monitored to maximize the IR camera frame-rate for the high loading-rate tests. More information about the camera acquisition parameters and the image analysis will be given in Section 2.3. At last, the synchronization of each measurement system and the data acquisition are performed by means of a Dewetron DEWE-2600 acquisition system at 1 MHz. For each configuration *i.e* every stacking sequences and loading rates, a minimum of three tests is performed in order to evaluate discrepancies between tests.

2.3 Crack detection based on infrared thermography for dynamic loadings

The protocol used in this study is based on a detection procedure which has been proposed by Berthe and Ragonet (Berthe et al. 2018). The extension of this methodology to thinner 90° plies and to higher loading rates will be studied in the sequel. The crack detection using an infrared camera relies on the fact that the occurence of some dissipative mechanisms such as matrix cracking leads to a local modification of the infrared radiation of the observed body. This modification associated to the local heat dissipation of the mechanism is directly related to a local temperature variation. A pixel-by-pixel calibration may be performed in order to conduct an accurate and a quantitative measurement as in Berthe's works, where one hundred images of a black body surface were captured every 0.5℃ between 20℃ and 29℃. In this study, we use the Telops pre-calibration which is valid for the Janos Asio 50 mm lens over the wavelength 3-5 µ and defined over a temperature range between 0℃ and 178℃ and for various integration times. In this study, the objective is not to obtain an accurate measurement of the absolute temperature, as the detection technique is only based on a sudden increase of the local temperature (at least 1°C) due to crack appearance. Consequently, the manufacturer calibration is accurate enough for the purpose of this study.

The following section aims at describing the methodology employed in order to objectively quantify the evolution of crack density from quasi-static to intermediate dynamic loadings. Following the first section, an illustration of the principle is presented for the $[0/90_2]_S$ configuration. The next section is referred to the results obtained at different strain rates and for several specimen thicknesses.

3 Results and discussions

3.1 Application to the $[0/90_2]_S$ configuration

3.1.1 Application on a tensile test performed at 5 mm.min^{-1}

Following a set of several increasing levels of tensile loads applied on a $[0/90_2]_S$ specimen, the Figure 2 illustrates several thermal fields referring to an apparent temperature variation ΔT, which have been captured over the whole surface of the side of the specimen.

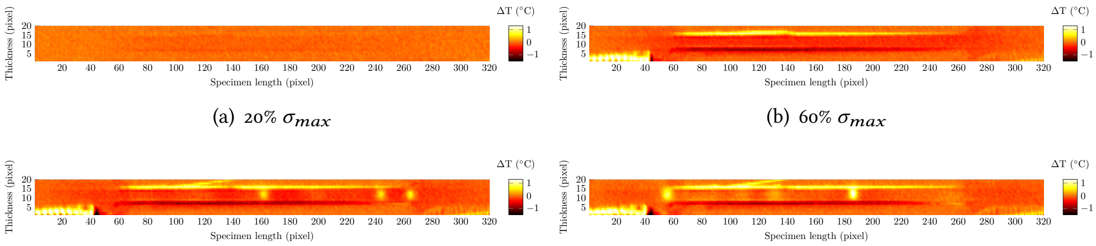

(a) 20% σ_{max}

(b) 60% σ_{max}

(c) 80% σ_{max}

(d) 95% σ_{max}

Figure 2: Evolution of the variation of the temperature ΔT captured along the edge of a $[0/90_2]_S$ laminate at several levels of load, for a test performed at 5 mm.min^{-1}

The fields of the apparent temperature variation are obtained by computing the difference of two temperature fields between a time t and the time t_0 which corresponds to the beginning of the loading of the sample. This analysis methodology is classically used by various authors to focus on temperature variation due to the mechanical loading of the sample (Meola et al. 2009; Portemont et al. 2018). At the beginning of the test, the abscissa within the intervals x = [0;60] and x = [265;320] refer to the tabs length. The abscissa within the interval x =]60;265[refers to the whole free-length of the specimen. The ordinates within the interval y = [8;16] refer to the specimen thickness of the free-length, which include both the two 0° plies on the outer faces of the specimen and the four 90° plies. The specimen is submitted to an uniaxial tensile load at the lower speed of this study (5 mm.min^{-1}). The acquiring frequency of the measuring load is about 10 kHz. The integration time of the infrared camera is set at 190µ. For a 320×20 pixels picture, the IR camera frequency is defined at 500 Hz. Considering this picture configuration, a set of five pixels through the thickness of the 90° plies are used to capture the crack mechanisms.

In the first instance and due to the thermoelasticity phenomenon, an homogeneous decrease of the apparent temperature is observed over the whole free length (Figure 2(b)). With the increase of the load applied to the specimen, several strongly localized hot areas can be observed. Only located within the total thickness of the 90° plies, these hot spot areas captured by the IR camera reveal the energy dissipated as heat during the process of creation of the transverse cracking mechanism (Figures 2(c) and 2(d)). A dedicated methodology for the quantification of matrix crack density using IR thermal fields and over a wide range of quasi-static tensile loads has been proposed by Berthe et al. 2018. This procedure has been validated with a cross analysis of the qualitative detection of the thermal events over the time and the quantitative detection of the load signals oscillations captured by the piezoelectric load cell that have been generated by crack occurrences. The main drawback of this methodology is that it is fully based on a manual user-based analysis of the thermal fields. In order to make this analysis more robust and convenient, a more automatic procedure is proposed in this study. It is based on the tracking of the thermal events along a sole line of pixels during the whole test period. The line of pixel is choosen to be located in the middle of the 90° plies and encompasses the whole free length of the sample (Figure 3(a)). From the beginning of the test until a few millisecond seconds before the final failure, the Figure 3(b) depicts every recorded occurrences related to each temperature variations along the line. It can be observed that most of captured thermal events are of the same amplitude and are diffusely spread over the entire free length with a relative constant distance between each peak. In order to consistently correlate the occurrence of thermal events with a level of applied stress, a time synchronization is required. Since the brittle failure of the samples results in the release of an high amount of energy, the failure phenomenon is objectively detectable on infrared images. The time synchronization is therefore based on the specimen final failure. The Figure 4 provides a representative result of the proposed methodology. As it can be seen, each crack occurrence can be directly related to the stress applied on a continuous basis.

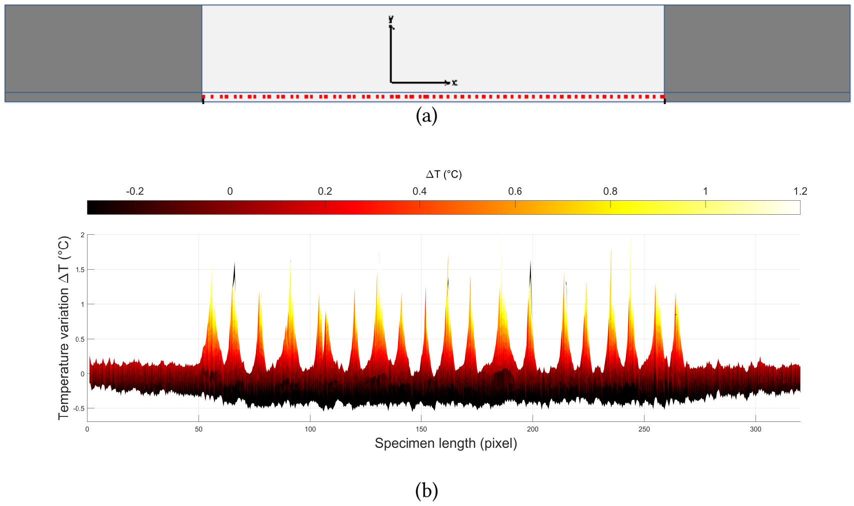

Figure 3: a) Schematic representation of a tracked line of pixels (red dots) located in the middle of the specimen thickness and within the 90° oriented plies, b) Captured thermal events along a line of a 320 pixel-length during a tensile test performed on a $[0/90_2]_S$ laminate at 5 mm.min^{-1}

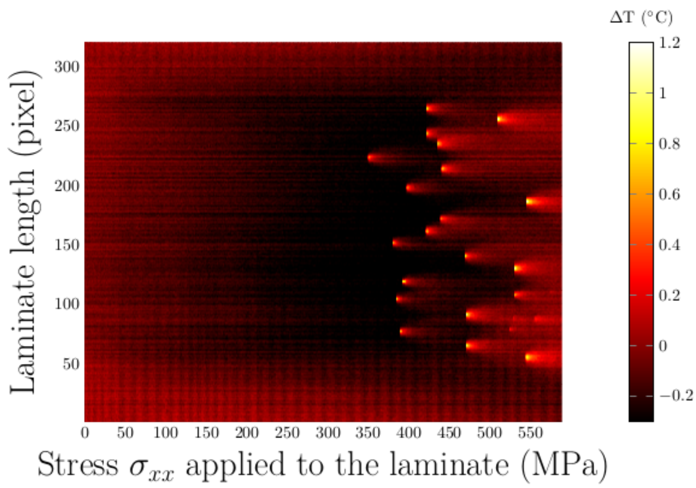

Figure 4: Spatial repartition of the thermal events directly related to the applied stress for a test performed at 5 mm.min^{-1} in a $[0/90_2]_S$ laminate

Another advantage related to this method lies in the direct access to a sole and explicit visualization of the spatial distribution of the cracks location from the beginning of the loading until the end. Concerning the considered stacking sequence and the considered loading speed, the first cracks appears for a longitudinal loading σ_{xx} = 349 MPa. Beyond this stress level, various cracks are generated within the free-length. As it can be also observed, the cracks still develop until the end of loading, which means that the crack kinematic has not reached its saturation level. In order to avoid the time-consuming nature of a manual crack count and to allow an objective quantification of crack density, an additional post-processing of the thermal pictures can be performed. A regularization of the ΔT fields can be performed using an unidirectional gradient over the time. The Figure 5(a) depicts the mean fields of the ∇ΔT in function of the applied stress, where the upper and lower bounds correspond to ten times the standard deviation of the ∇ΔT mean. By reducing the noise around the thermal events, the cracking mechanism is emphasized and can be accurately detected by means of an automatized peaks detection subroutine. Based on this methodology, accurate evolution laws of crack density can be obtained and illustrated as in Figure 5(b). The crack density is computed by means of the Equation 1:

$$d = \frac{N_c}{l_0} \tag{1}$$

with N_c the number of transverse cracks counted in the 90° plies. A reliable applied stress is obtained for each generated cracks. For the three performed tests, this procedure leads to low discrepancies results, with a mean value of σ_{onset} = 383 MPa ± 30 MPa regarding the stress threshold of the crack onset. The evolution of the crack kinetics is found to be similar between the three tests. A mean value of the

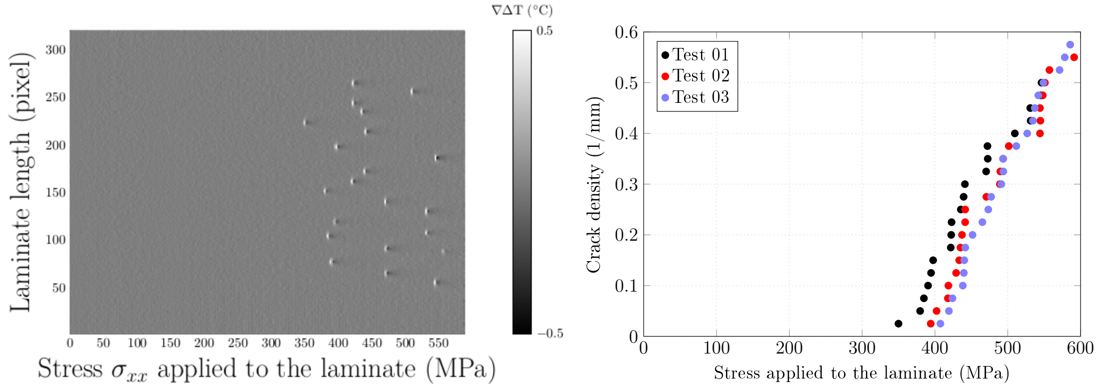

(a) (b)

Figure 5: Cracks density d based on crack detection in infrared thermography images: a) Regularized thermal field as a function of the applied stress for the Test 01 and b) Quantification of the evolution of the crack density for the three tests performed at 5 mm.min^{-1}

maximum crack density $d_{\max} = 0.54 \pm 0.04$ is obtained for an average $\sigma_{xx}^{d\max} = 574.42 \pm 24.5$ MPa. A mean value of $\sigma_{xx} = 602.45$ MPa $\pm$ 11.9 MPa is measured for the maximum stress applied to the laminate.

3.1.2 Application on tensile tests performed at several loading rates

One of the main objective of the study is to assess the reliability of the proposed methodology to be applied for high speed tensile tests. As mentioned in Section 2.2, five loading speeds are considered. For each considered loading speed and each stacking sequence configuration, the infrared camera parameters are summarised in Table 1 as well as the induced uncertainty associated with the crack occurence detection.

Loading rates	Resolution (pixels)	Integration time (μ)	IR Frame-rate (Hz)	Time uncertainty (s)	Stress uncertainty (MPa)
5 mm.min^{-1}	320 × 20	190	500	2 ×10^{-3}	≤ 0.1
50 mm.min^{-1}	320 × 20	180	4000	2.5 ×10^{-4}	≤ 0.2
500 mm.min^{-1}	256 × 16	180	5000	2 ×10^{-4}	≤ 0.7
0.1 m.s^{-1}	256 × 16	180	5000	2 ×10^{-4}	≤ 7
1.4 m.s^{-1}	256 × 12	60 - 15	15000 - 30000	6.7 ×10^{-5} - 3.4 ×10^{-4}	≃ 50

Table 1: Parameters of the infrared camera used for the whole experimental investigation from static to intermediate dynamic loadings

It can be noticed that the integration time remains overall constant regardless of the loading rate. To reach a higher acquisition frequency for the test performed at 1.4 m.s^{-1}, the integration time for these tests has to be reduced. An integration time of 15μ is used for the $[0/90_3]_S$ and $[0/90_2]_S$ laminate configurations. An integration time of 60μ is used for the thinner laminate configurations $[0/90_1]_S$ and $[0/90_{1/2}]_S$ to increase the sensitivity of the measurement for these configuration where crack detection can be more difficult. Based on the procedure described in Section 3.1.1, the Figures 6, 7, 8 and 9 are used to illustrate the capability of the protocol to capture and to quantify crack mechanisms over a large range of strain rates regarding the $[0/90_2]_S$ laminate configuration. It should be mentioned that although a reduction in spatial resolution is required for high-speed loadings, the number of effective pixels in the thickness of the 90° layers remains fixed at 5 pixels. First of all, the Figures 6(a), 7(a), 8(a) and 9 illustrate the ability of the experimental protocol to capture the cracking mechanism and to associate it directly with the applied stress is demonstrated over a wide range of quasi-static and dynamic loading rates. For the last loading rate considered in this study, although it is possible to qualitatively capture the presence and the spatial distribution of the cracking mechanism, the low temporal sampling (only 5 images for the whole loading) does not allow a continuous and consistent quantification of the cracking kinetics. This loading rate is therefore withdrawn for the rest of the analysis in the sequel of the study. This loading rate can be considered as a limit of this experimental investigation due to the current acquiring frequency of IR cameras. On the other hand, the Figures 6(b), 7(b) and 8(b) clearly exhibits that a relatively low scattering of the experimental results can be observed. It can also be noticed that the spatial cracks distribution seems to be unaffected by the loading rate increase. The cracks are still spread through the free length in a random way. The Table 2 allows to quantitatively describes the evolution of the considered mechanism. The results exhibit a very low scatter regarding the maximum crack density and the stress level corresponding to the

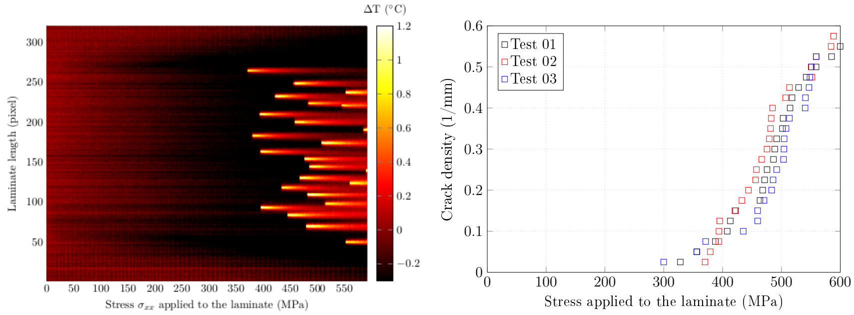

(a) Captured thermal events for Test 02 (b) Crack kinetics

Figure 6: Crack density related to the applied stress for a $[0/90_2]_S$ laminate submitted to tensile tests performed at 50 mm.min^{-1}.

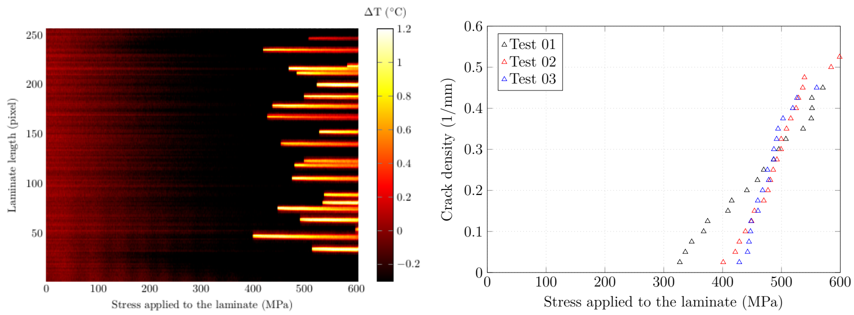

(a) Captured thermal events for Test 02 (b) Crack kinetics

Figure 7: Crack density related to the applied stress for a $[0/90_2]_S$ laminate submitted to tensile tests performed at 500 mm.min^{-1}.

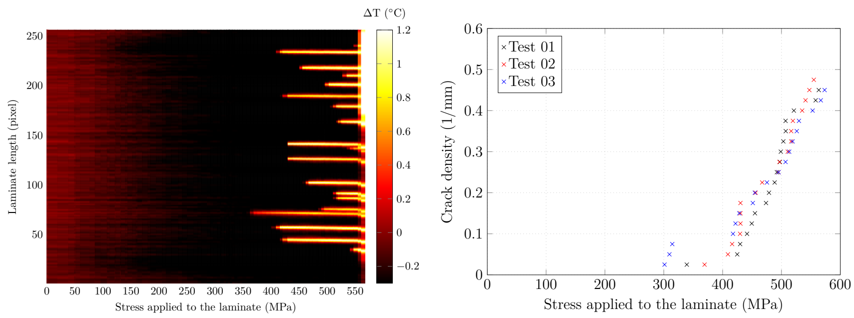

(a) Captured thermal events for Test 02 (b) Crack kinetics

Figure 8: Crack density related to the applied stress for a $[0/90_2]_S$ laminate submitted to tensile tests performed at 0.1 m.s^{-1}.

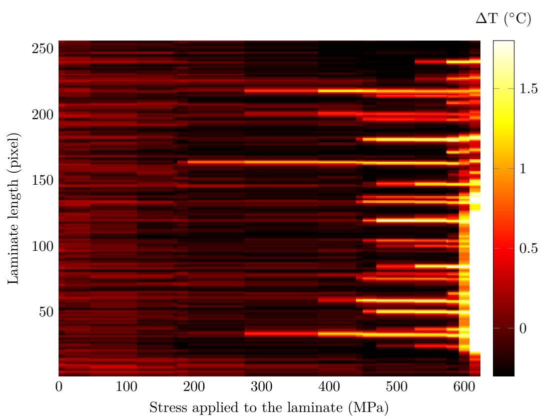

Figure 9: Captured thermal events for a $[0/90_2]_S$ laminate submitted to tensile tests performed at 1.4 m.s^{-1}.

Loading rates	σ_{onset} (MPa)	d^{max} (mm^{-1})	$\sigma_{xx}^{d^{max}}$ (MPa)
5 $mm.min^{-1}$	383.9 ± 7.83%	0.54 ± 0.04	574.42 ± 4.30%
50 $mm.min^{-1}$	332.7 ± 10.63%	0.55 ± 0.03	582.47 ± 3.62%
500 $mm.min^{-1}$	385.5 ± 13.5%	0.50 ± 0.04	590.58 ± 4.65%
0.1 $m.s^{-1}$	336.6 ± 10.1%	0.46 ± 0.02	563.92 ± 1.63%

Table 2: Crack kinetics results using the IR thermal protocol for the $[0/90_2]_S$ laminate at several loading rates

last detected crack. As expected, a larger scattering is observed for the stress threshold at the onset of the first crack. Similarly to the thicker laminates tested up to 500 $mm.min^{-1}$ in Berthe et al. 2018, no rate effects seem to emerge for this stacking sequence over the same range of loading rate and up to 0.1 $m.s^{-1}$.

The methodology described in this section presents therefore the benefits of being simple from a post-processing point of view and for the interpretation of the data. The reliability of the procedure has been demonstrated over a wide range of loading rates. Moreover, this methodology gives access to a continuous measurement correlated to the spatial distribution of the cracks as a function of the stress applied to the specimen at several loading rates which can be useful for the validation of the constitutive laws. In the sequel, the same procedure is applied to the other three laminate configurations in order to assess the capability of the presented methodology to be applied to different cross-ply laminate thicknesses.

3.2 Influence of the ply thickness on the rate dependency of crack density evolution

Based on the experimental protocol and the previously presented methodology, the influence of 90° ply thickness on the rate effect of the transverse crack kinetics is assessed. First of all, the results obtained with the thinner $[0/90_{1/2}]_S$ laminate configuration have been proven to be the current limit of this protocol due to the experimental setup and camera configuration chosen for this experimental investigation. Indeed an insufficient amount of pixels (*i.e.* 1 pixel) located in the thickness of the 90° ply is obtained with the selected free-length and camera's lens. This low spatial resolution does not ensure a consistent detection of the crack occurrences, hence the thinner configuration considered in this study is withdrawn of the following analysis. By using samples of smaller free-length and another camera lens, the spatial resolution can be increased and this limitation might be overcome. Despite this limitation, the Figure 10 and Figure 11 illustrate the results from the proposed procedure applied to the configurations $[0/90_3]_S$ at 0.1 $m.s^{-1}$ and $[0/90_1]_S$ for each loading-rates, where the number of pixels in the thickness of the 90° plies is fixed at 9 pixels and 3 pixels respectively, regardless of the considered loading rate for this study. As it can be

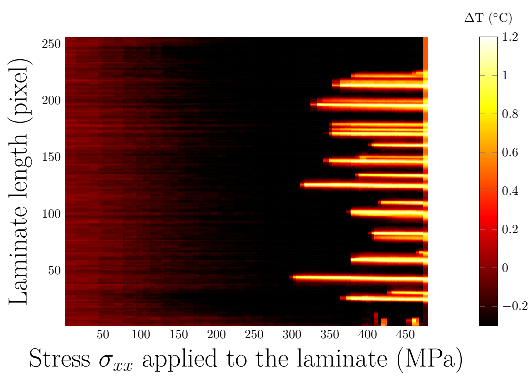

Figure 10: Captured thermal events for a $[0/90_3]_S$ laminate submitted to a tensile test performed at 0.1 $m.s^{-1}$

observed, the crack mechanism remains well captured for the both laminate configurations over the whole range of loading rates. With the method proposed in this paper, a direct comparison between the thicker and the thinner laminate configurations can be established. As it can be qualitatively observed, the more the decrease in the number of 90° plies, the more the crack density and the stress threshold regarding the onset of the first crack. These trend is quantitatively depicts in the Figure 12 where every tensile tests performed at a loading rate of 5 $mm.min^{-1}$ are reported for each tested laminate configuration. For the $[0/90_3]_S$ configuration, the results used in this study for the loading rates between 5 $mm.min^{-1}$ and 500 $mm.min^{-1}$ are extracted from Berthe et al. 2018. For the thickest configuration, the average of the

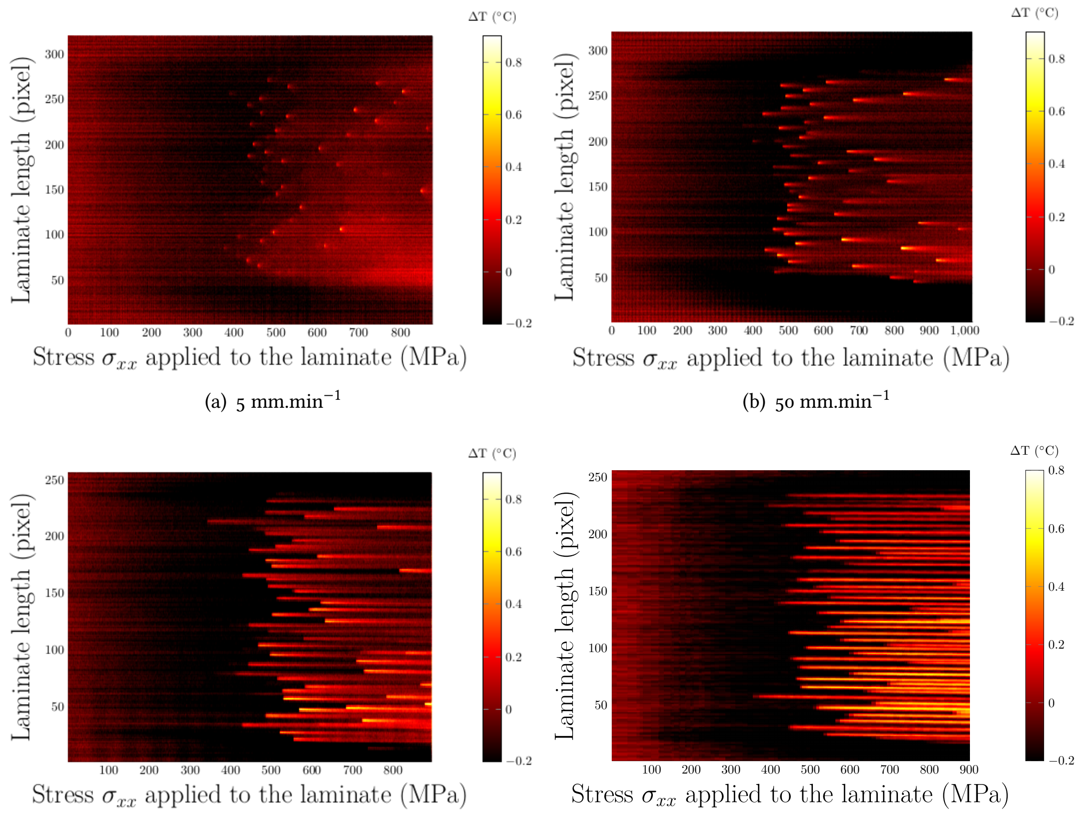

(a) 5 mm.min^{-1} (b) 50 mm.min^{-1} (c) 500 mm.min^{-1} (d) 0.1 m.s^{-1}

Figure 11: Captured thermal events for a $[0/90_1]_S$ laminate submitted to tensile tests performed at several loading rates.

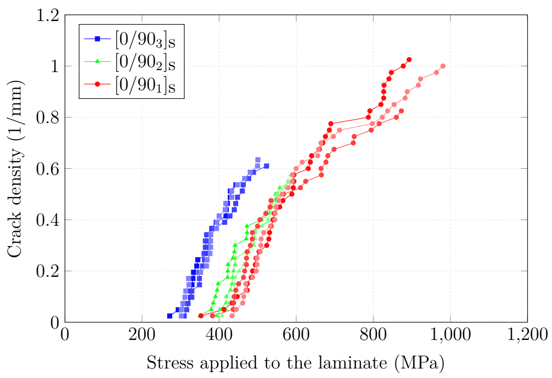

Figure 12: Thickness effect on the crack density captured with the IR protocol and based on tensile tests performed at 5 mm.min^{-1}.

maximum crack density is estimated at d^{max} = 0.59 ± 0.05 upon reaching an average mean stress value estimated at $\sigma_{xx}^{d\max}$ = 488.96 MPa ± 8.37% and a stress threshold for crack onset at a mean value of about σ_{onset} = 294.37 MPa ± 6.73%. For the thinnest configuration, the average of the maximum crack density is estimated at d^{max} = 0.95 ± 0.11 upon reaching an average mean stress value estimated at $\sigma_{xx}^{d\max}$ = 915.33 MPa ± 6.27% and a stress threshold for crack onset at a mean value of about σ_{onset} = 389.62 MPa ± 10.45%. On the other hand, the intermediate $[0/90_2]_S$ laminate configuration is consistently located between the two others although it can be seen that the maximum crack density appears to be slightly lower than the thicker configuration. Finally, these trends are in agreement with those reported in Parvizi et al. 1978; Nairn et al. 2000; Berthelot 2003, which increases the confidence in the proposed IR thermal detection protocol.

The loading rate sensitivity is analysed in the sequel. The stress–strain responses for the different loading rates considered in this study are plotted in Figure 13. For the three different laminate configurations, these figures include each of the three tests performed for each loading rate in order to assess the low

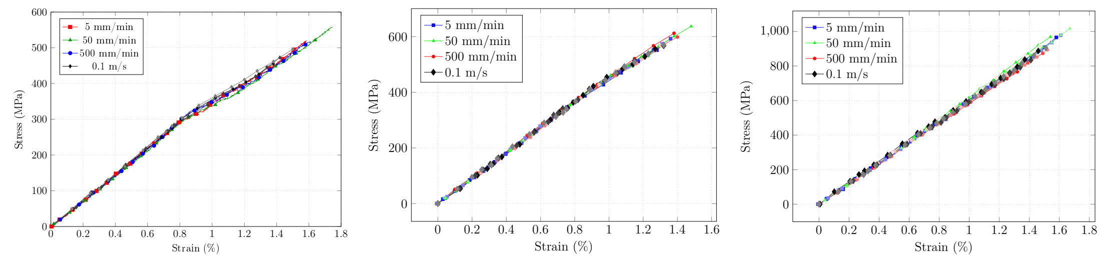

(a) $[0/90_3]_S$ (b) $[0/90_2]_S$ (c) $[0/90_1]_S$

Figure 13: Macroscopic tensile behavior of the three laminate configurations at several loading rates.

experimental scattering. On the one hand, no rate effect is clearly emphasized regarding the macroscopic behavior over the considered range of loading rates. On the other hand and as expected, the lower the number of 90° plies, the greater macroscopic failure stress. Respectively to each laminate configuration, the failure stress can be considered as rate-insensitive. These two aspects suggest that most of the mechanical contribution to the macroscopic behavior for these cross-ply configurations can be attributed to the outer 0° plies, whose rate-insensitivity is well known. Finally, the crack density evolution with respect to the applied stress is plotted for the different loading rates and for each laminate configuration in Figure 14. This figure includes the three different tests performed for each loading rate in order to assess

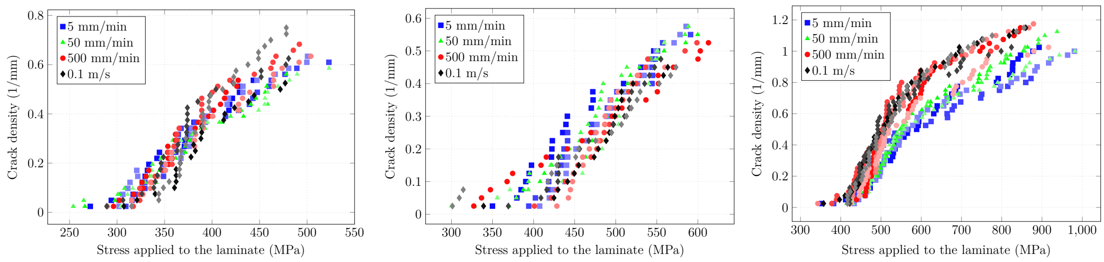

(a) $[0/90_3]_S$ (b) $[0/90_2]_S$ (c) $[0/90_1]_S$

Figure 14: Quantified crack density for the three laminate configurations at several loading rates.

the low experimental scattering. As it can be observed in the Figure 14(a) and Figure 14(b), the crack density and its kinetic appear to be rate-insensitive over the wide range of loading rates considered in this paper. On the contrary, the Figure 14(c) clearly exhibits a rate dependency of the transverse cracking evolution. For the $[0/90_1]_S$ laminate, the crack density evolution appears to be accelerated particularly between σ_{xx} = 400 MPa and σ_{xx} = 500 MPa with the loading rate increase. Consequently, the maximum crack density reaches a higher value for the two higher loading rates (*i.e.* 500 mm.min^{-1} and 0.1 m.s^{-1}) than for the two lower loading rates (*i.e.* 5 mm.min^{-1} and 50 mm.min^{-1}). We can finally notice that the higher the loading rate, the lower the $\sigma_{xx}^{d\max}$. It can be concluded that the thickness of cross-ply laminate have a significant influence on the rate effect of the transverse cracking mechanism. In spite of this conclusion and on the contrary with Nguyen et al. 2015, the stress at which the first crack appeared appears to be rate-insensitive in this study. The quantitative synthesis of these trends is illustrated in Table 3.

3.3 Discussions

On the first hand, the origin of the emphasized loading-rate effect on the thinner stacking sequence might be explained from an energetic point of view. As firstly observed by Parvizi (Parvizi et al. 1978) regarding cross-ply glass fiber reinforced polymers and well summarized by Leguillon (Leguillon 2002), as long as the 90° ply thickness remains sufficiently thick, the onset of the transverse cracking occurrence appears for a constant strain and could be predict with a stress criterion based on a constant stress value. Below a critical thickness, the applied stress must be increased and a stress criterion for the onset of crack occurrence cannot be longer considered consistent compared to an energy criterion based on the mode I fracture toughness G_c. A considerable amount of work has been performed regarding the rate dependency of the G_c fracture toughness Yaniv 1987; Hug et al. 2006; Isakov et al. 2019; Azadi et al. 2019, although there is no consensus regarding its rate dependency. This is mainly due to the fact that the G_c characterisation tests are not normalized for high speed loading May 2016 leading to inconsistency trends for which results are highly dependent on the protocol. In order to nonetheless develop the line of reasoning, we note that some studies conclude that increasing loading rates would lead to a decrease in G_c

$[0/90_3]_S$ Loading rates	Strain-rate $\dot{\varepsilon}$ (s^{-1})	σ_{onset} (MPa)	d^{max} (mm^{-1})	$\sigma_{xx}^{d_{max}}$ (MPa)
5 $mm.min^{-1}$	8.3×10^{-4}	294.4 ± 6.74%	0.59 ± 0.05	488.96 ± 8.37%
50 $mm.min^{-1}$	6.4×10^{-3}	274.7 ± 9.50%	0.53 ± 0.08	486.59 ± 6.79%
500 $mm.min^{-1}$	4.6×10^{-2}	301.0 ± 4.76%	0.62 ± 0.07	474.40 ± 8.66%
0.1 $m.s^{-1}$	0.78	303.9 ± 4.38%	0.63 ± 0.11	478.56 ± 0.38%
$[0/90_2]_S$ Loading rates	Strain-rate $\dot{\varepsilon}$ (s^{-1})	σ_{onset} (MPa)	d^{max} (mm^{-1})	$\sigma_{xx}^{d_{max}}$ (MPa)
5 $mm.min^{-1}$	8.1×10^{-4}	383.9 ± 7.83%	0.54 ± 0.04	574.42 ± 4.30%
50 $mm.min^{-1}$	6.5×10^{-3}	332.7 ± 10.63%	0.55 ± 0.03	582.47 ± 3.62%
500 $mm.min^{-1}$	4.0×10^{-2}	385.5 ± 13.5%	0.50 ± 0.04	590.58 ± 4.65%
0.1 $m.s^{-1}$	0.79	336.6 ± 10.1%	0.46 ± 0.02	563.92 ± 1.63%
$[0/90_1]_S$ Loading rates	Strain-rate $\dot{\varepsilon}$ (s^{-1})	σ_{onset} (MPa)	d^{max} (mm^{-1})	$\sigma_{xx}^{d_{max}}$ (MPa)
5 $mm.min^{-1}$	9.1×10^{-4}	389.6 ± 10.45%	0.95 ± 0.11	915.33 ± 6.27%
50 $mm.min^{-1}$	7.5×10^{-3}	424.2 ± 1.83%	1.04 ± 0.04	912.37 ± 6.78%
500 $mm.min^{-1}$	4.1×10^{-2}	381.5 ± 10.5%	1.12 ± 0.08	878,84 ± 5.53%
0.1 $m.s^{-1}$	0.79	398.9 ± 9.0%	1.11 ± 0.07	846.42 ± 2.30%

Table 3: Synthesis of the crack kinetics results using the IR thermal protocol for each laminate configurations and each loading rates

Kusaka et al. 1998; Zabala et al. 2015; Thorsson et al. 2018. Considering this aspect, Laws et al. 1988 has shown, by means of an analytical prediction, that the tougher the material the less the crack density (see Figure 15). Consequently, the decrease of G_c with the loading rate increase may explain the maximum crack density increased d^{max} and the associated $\sigma_{xx}^{d_{max}}$ decreased.

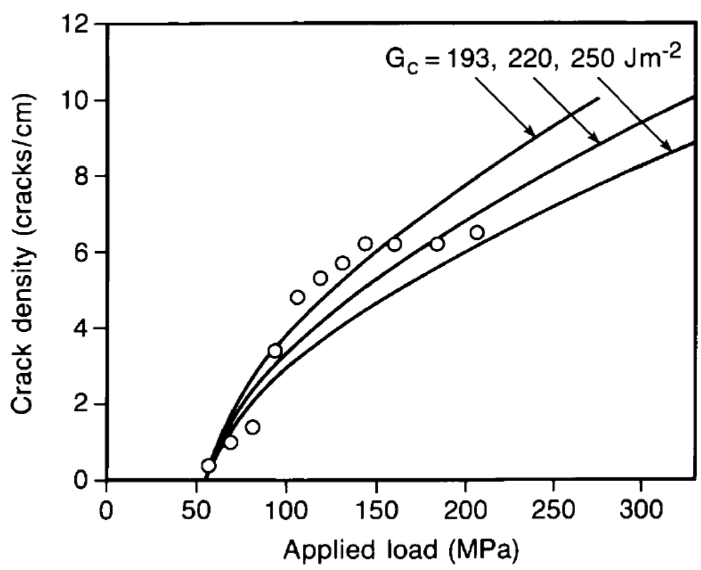

Figure 15: Prediction of the progressive cracking in a $[0/90_3]_S$ E-glass epoxy laminates for several values of G_c (Laws et al. 1988).

On the other hand, a loading rate effect can also be observed on the thicker configuration. With the loading rate increase, the shape of the observed cracks evolves and curved/oblique cracks can be observed for the higher loading speed as shown in Figure 16. Curved cracks classically appear when the 90° ply thickness increase Groves et al. 1987; Allen et al. 1988. Only few studies deal with this specific mechanism. Nevertheless, it would seem that this phenomenon might be linked and appear as consequence to the saturation of the transverse cracking mechanism Hu et al. 1993 or due to the difference in toughness between mode I and mode II for a given material Jalalvand et al. 2014. In this study, curved cracks appear for the configuration with six 90° plies but only for higher loading rates. This phenomenon might also be a consequence of a material rate dependency which is observed for this configuration on the matrix cracking

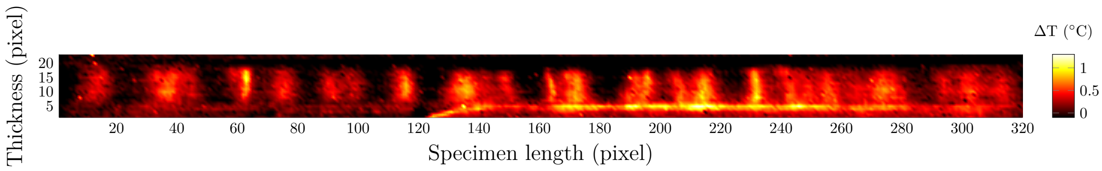

(a) 500 mm.min−1

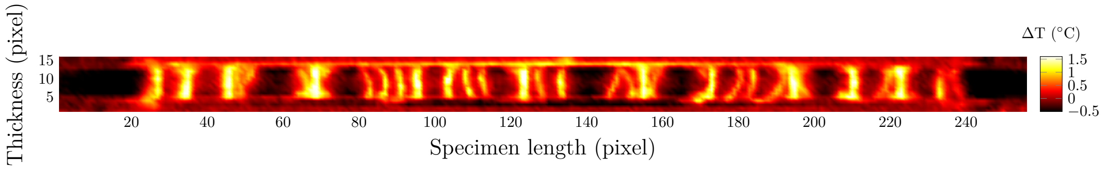

(b) 0.1 m.s^{-1}

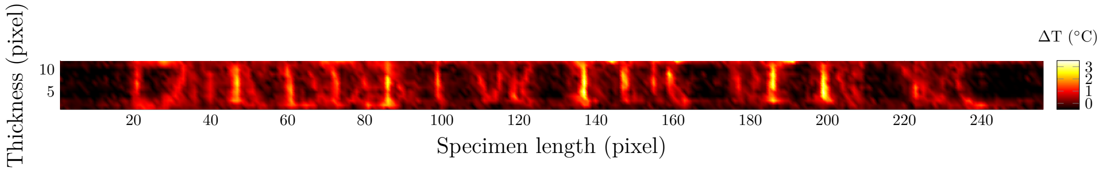

(c) 1.4 m.s^{-1}

Figure 16: Illustration of the transverse cracking pattern on a $[0/90_3]_S$ laminate prior the final failure of the specimen submitted at several loading rates.

pattern and no longer observed on matrix crack density evolution.

4 Conclusions

This study firstly aimed at assessing the experimental capability of an infrared thermal protocol to capture and accurately quantify the evolution of transverse matrix cracking in cross-ply laminates submitted to various loading rates from quasi-static to intermediate loading rates. On the other hand, different laminate thicknesses have been considered in order to assess the influence of the 90° plies on the rate dependency of the crack mechanism. This study has allowed to validated the use of the proposed protocol for detecting the matrix cracking mechanism by infrared thermography over the wide range of loading rates. By means of a simple analysis methodology of the thermal data, which has been proven to be valid whatever the loading rate, it is possible to get access to an objective and an accurate representation of the evolution of the crack density over the whole free length of the specimen and directly as a function of the applied stress until the final failure. The trends associated with thickness effects in this study are in agreement with the literature. Focusing on the studied material and the considered range of loading rates, this study emphasises that a rate dependency of the crack density evolution with respect to the applied stress can be observed only for the $[0/90_1]_S$ laminate. For this configuration, the increase of the loading rate leads to an increase of the maximum crack density without affecting the onset threshold of the mechanism. The observed rate dependency has to be further investigated in order to better understand the threshold effect driven by 90° ply thickness observed in this study and leading to an observable rate dependency of the matrix crack density evolution.

Acknowledgments

The authors gratefully acknowledge the funding from the French Civil Aviation Directorate (DGAC). They also gratefully acknowledge the Hauts-de-France Region for funding equipment that contributed to this research work.

5 Bibliography

Allen, D., C. Harris, S. Groves, and R. Norvell (1988). “Characterization of Stiffness Loss in Crossply Laminates with Curved Matrix Cracks”. *Journal of Composite Materials* 22.1, pp. 71–80. doi: 10.1177/002199838802200105. eprint: https://doi.org/10.1177/002199838802200105

Azadi, M., M. Saeedi, M. Mokhtarishirazabad, and P. Lopez-Crespo (2019). “Effects of loading rate on crack growth behavior in carbon fiber reinforced polymer composites using digital image correlation technique”. *Composites Part B: Engineering* 175, pp. 107–161. doi: https://doi.org/10.1016/j.compositesb.2019.107161

Battams, G. (2014). “The use of optical techniques to assess the damage tolerance of composite materials”. PhD thesis. University of Southampton

Battams, G. and J. Dulieu-Barton (2016). “Data-rich characterisation of damage propagation in composite materials”. *Composites Part A: Applied Science and Manufacturing* 91, pp. 420–435

Berthe, J and M Ragonet (2018). “Passive infrared thermography measurement of transverse cracking evolution in cross-ply laminates”. *Strain* 54.6

Berthelot, J.-M. (2003). “Transverse cracking and delamination in cross-ply glass-fiber and carbon-fiber reinforced plastic laminates: static and fatigue loading”. *Applied Mechanics Reviews* 56.1, pp. 111–147

Crossman, F., W. Warren, A. Wang, and J. G.E. Law (1980). “Initiation and Growth of Transverse Cracks and Edge Delamination in Composite Laminates Part 2. Experimental Correlation”. *Journal of Composite Materials* 14.1, pp. 88–108. doi: 10.1177/002199838001400107. eprint: https://doi.org/10.1177/002199838001400107

Dzenis, Y. (2003). “Cycle-based analysis of damage and failure in advanced composites under fatigue: 1. Experimental observation of damage development within loading cycles”. *International Journal of Fatigue* 25.6, pp. 499 –510. doi: https://doi.org/10.1016/S0142-1123(02)00170-6

Farge, L., J. Varna, and Z. Ayadi (2010). “Damage characterization of a cross-ply carbon fiber/epoxy laminate by an optical measurement of the displacement field”. *Composites Science and Technology* 70.1, pp. 94 –101. doi: https://doi.org/10.1016/j.compscitech.2009.09.010

Groves, S. E., C. E. Harris, A. L. Highsmith, D. H. Allen, and R. G. Norvell (1987). “An experimental and analytical treatment of matrix cracking in cross-ply laminates”. *Experimental Mechanics* 27.1, pp. 73–79. doi: 10.1007/BF02318867

Hu, S., J. S. Bark, and J. A. Nairn (1993). “On the phenomenon of curved microcracks in [(S)/90n]s laminates: Their shapes, initiation angles and locations”. *Composites Science and Technology* 47.4, pp. 321 –329. doi: https://doi.org/10.1016/0266-3538(93)90001-W

Huchette, C. (2005). “Sur la complémentarité des approches expérimentales et numériques pour la modélisation des mécanismes d’endommagement des composites stratifiés”. PhD thesis. Paris 6

Hug, G., P. Thevenet, J. Fitoussi, and D. Baptiste (2006). “Effect of the loading rate on mode I interlaminar fracture toughness of laminated composites”. *Engineering Fracture Mechanics* 73, pp. 2456–2462

Isakov, M., M. May, P. Hahn, H. Paul, and M. Nishi (2019). “Fracture toughness measurement without force data. Application to high rate DCB on CFRP”. *Composites Part A: Applied Science and Manufacturing* 119, pp. 176 –187. doi: https://doi.org/10.1016/j.compositesa.2019.01.030

Jalalvand, M., M. R. Wisnom, H. Hosseini-Toudeshky, and B. Mohammadi (2014). “Experimental and numerical study of oblique transverse cracking in cross-ply laminates under tension”. *Composites Part A: Applied Science and Manufacturing* 67, pp. 140 –148. doi: https://doi.org/10.1016/j.compositesa.2014.08.004

Kusaka, T., M. Hojo, Y.-W. Mai, T. Kurokawa, T. Nojima, and S. Ochiai (1998). “Rate dependence of mode I fracture behaviour in carbon-fibre/epoxy composite laminates”

Laws, N. and G. Dvorak (1988). “Progressive transverse cracking in composite laminates”. *Journal of Composite Materials* 22, pp. 900–916

Leguillon, D. (2002). “Strength or toughness? A crirerion for crack onset a a notch”. *European Journal of Mechanics* 21, pp. 61–72

Li, Y., Z. wei Yang, J. tang Zhu, A. bo Ming, W. Zhang, and J. yu Zhang (2016). “Investigation on the damage evolution in the impacted composite material based on active infrared thermography”. *NDT & E International* 83, pp. 114 –122. doi: https://doi.org/10.1016/j.ndteint.2016.06.008

Lisle, T., C. Bouvet, P. M.L., P. Margueres, and R. Prieto Corral (2013). “Damage analysis and fracture toughness evaluation in a thin woven composite laminate under static tension using infrared thermography”. *Composites Part A: Applied Science and Manufacturing* 53, pp. 75–87

May, M. (2016). “Measuring the rate-dependant mode I fracture toughness of composite - A review”. *Composites: Part A* 81, pp. 1–12

Meola, C. and G. M. Carlomagno (2009). “Infrared thermography of impact-driven thermal effects”. *Applied Physics A* 96.3, pp. 759–762

Mian, A., X. Han, S. Islam, and G. Newaz (2004). "Fatigue damage detection in graphite/epoxy composites using sonic infrared imaging technique". *Composites Science and Technology* 64.5, pp. 657 –666. doi: https://doi.org/10.1016/j.compscitech.2003.07.005

Montesano, J., H. Bougherara, and Z. Fawaz (2014). "Application of infrared thermography for the characterization of damage in braided carbon fiber reinforced polymer matrix composites". *Composites Part B: Engineering* 60, pp. 137 –143. doi: https://doi.org/10.1016/j.compositesb.2013.12.053

Nairn, J., R Talreja, and J. Manson (2000). "Polymer matrix composites". *Comprehensive composite materials.* Vol. 2. Elsevier Science, pp. 403–432

Nguyen, T. and D. Gamby (2015). "Loading rate effect on matrix transverse cracking in aeronautical CFRP composite laminates"

Parvizi, A., K. Garret, and J. Bailey (1978). "Constrained cracking in glass fibre reinforced epowy cross-ply laminates". *Journal of Materials Sience* 195-201, pp. 195–201

Portemont, G., J. Berthe, A. Deudon, and F.-X. Irisarri (2018). "Static and dynamic bearing failure of carbon/epoxy composite joints". *Composite Structures* 204, pp. 131–141

Talreja, R. (1985). "Transverse cracking and stiffness reduction in composite laminates". *Journal of Composites Materials* 4, pp. 355–375

Thorsson, S. I., A. M. Waas, J. Schaefer, B. Justusson, and S. Liguore (2018). "Effects of elevated loading rates on mode I fracture of composite laminates using a modified wedge-insert fracture method". *Composites Science and Technology* 156, pp. 39 –47. doi: https://doi.org/10.1016/j.compscitech.2017.12.018

Toubal, L., M. Karama, and B. Lorrain (2006). "Damage evolution and infrared thermography in woven composite laminates under fatigue loading". *International Journal of Fatigue* 28.12, pp. 1867 –1872

Yaniv G.and Daniel, I. M. (1987). "Composite Materials Testing and Design 8th Conference". *ASTM STP972, American Society for Testing and Materials: Philadelphia*

Zabala, H., L. Aretxabaleta, G. Castillo, and J. Aurrekoetxea (2015). "Loading rate dependancy on mode I interlaminar fracture toughness of unidrectional and woven carbon fibre epoxy composites". *Composites Structures* 121, pp. 75–82